

We are IntechOpen, the world's leading publisher of Open Access books Built by scientists, for scientists

6,900

Open access books available

185,000

International authors and editors

200M

Downloads

Our authors are among the

154

Countries delivered to

TOP 1%

most cited scientists

12.2%

Contributors from top 500 universities



WEB OF SCIENCE™

Selection of our books indexed in the Book Citation Index
in Web of Science™ Core Collection (BKCI)

Interested in publishing with us?
Contact book.department@intechopen.com

Numbers displayed above are based on latest data collected.
For more information visit www.intechopen.com



Treatment of Agro-Food Wastewaters and Valuable Compounds Recovery by Column Sorption Runs

Jacques Romain Njimou, Fridolin Kouatchie Njeutcha, Emmanuel Njungab, André Talla and Nkeng George Elambo

Abstract

Olive oil extraction generates a large quantity of wastewater which is a strong pollutant due to its high organic load and phytotoxic. However, its content in antibacterial phenolic substances displays to be resistant to biological degradation. The discharge of olive mill wastewater (OMWW) is not allowed through the municipal sewage system and/or in a natural effluent. Unfortunately, the current technologies for the treatment of OMWW are expensive and complicated to be operated in a mill factory where the objective of this study. We have designed and implemented a process that permitted both the treatment of agro-food processing water and the recovering of compounds of market interest. The process was applied in the effluents of olive oil mill factories to recover polyphenols with a possible significant reduction of organic waste. The nanofiltration fraction obtained from a sequential treatment involved coagulation, photocatalysis, ultrafiltration and nanofiltration was performed to separate the most valuable compounds using column adsorption runs. Competitive adsorption and the selectivity were obtained for phenol and hydroxytyrosol onto macro-reticular aromatic polymer (FPX66) and macroporous polystyrene cross-linked with divinylbenzene (MN202), respectively. The investigations were followed by a single component of phenol or tyrosol, binary phenol and tyrosol and ternary components in NF concentrate of OMWW for valuable compounds recovery conducted in a fixed-bed adsorber of resins. During the intermediate stage of the column operation, adsorbed tyrosol molecules were replaced by the incoming phenol molecules due to the lower tyrosol affinity for FPX66 resin and the tyrosol concentration was higher than its feed concentration.

Keywords: OMWW, ultrafiltration, nanofiltration, fixed-bed column, polyphenols recovery, polymeric resins

1. Introduction

Phenol and phenolic species are chemicals commonly found in various industrial waste in general and in a particular in olive mill wastewater. Phenol is also known as

carbolic acid. It's a white crystalline toxic solid with a sweet tarry odor commonly referred to as a "hospital smell"; with a pKa of 9.98 and solubility of 8% (wt.) in the water at 25°C. In fact, the US Environmental Protection Agency (EPA) and the European Union (EU) directive number 80/778/EC consider phenol as a priority pollutant [1]. The concentration of phenol in wastes varies in a wide range from several ppm to 2–3% and phenols degradability are limited. Several techniques are available currently for the treatment of phenolic effluents.

Adsorption processes have been intensively used in wastewater treatment for phenol and other organic compounds. Phenols in olive mill wastewaters (OMWW) have very complex compositions and the treatment feasibility has to be separately made through experimental approaches [2–6]. Conventional fixed bed processes involve a saturation, adsorption or loading step, followed by desorption, elution or regeneration steps [7]. The use of granular activated carbon (GAC) for removing toxic organic chemicals including phenol from wastewater is one of the best commercially proven methods. Although activated carbons exhibit an excellent adsorption capacity for the removal of phenol from wastewater, this method exhibited the difficulty to its regeneration and quite expensive to dispose of [7–12].

Therefore, the necessity of the alternative adsorbents which are equally effective and easier to regenerate and recently, a new kind of hypercrosslinked polymeric adsorbent was found to be very effective for removing aromatic compounds from aqueous solutions [5, 7, 13, 14]. Macroreticular resins are the most promising in the separation processes due to its easier regeneration and it is well used in industrial practices. The wide variations in functionality, surface area, and porosity available for macroreticular resins present the possibility of its selective separation of the effective components. Furthermore, the regeneration of the resins can easily be accomplished with a solvent and hence, the adsorption of phenol can be realized by macroreticular resins. Numerous studies on the removal of metals and organic pollutants by these adsorbents in discontinuous systems have been reported [10, 11, 15]. However, the application in continuous systems i.e. in a fixed-bed column is often preferred, since it is simple to operate, given to high yields and can be scaled-up in the laboratory process. In order to design and operate fixed-bed adsorption process successfully, both equilibrium and dynamic adsorptions in specified systems must be known. The indicators are the breakthrough curves under specified operating conditions must be predictable. The shape of this curve is determined by the shape of the isotherm equilibrium and it is influenced by the individual transport processes in the column of adsorbent [10, 11, 15].

In this chapter, the experimental results on adsorption tests performed by resins were presented. The polyphenols are extracted from a nanofiltration concentrate stream produced during the purification of olive vegetation wastewater from a 3 phase process. This wastewater contains many polyphenols, mostly hydroxytyrosol, which may have a market.

The high organic content of olive wastewater exhibits to its impossible direct recovering of polyphenols content. The high suspended solids in the raw stream will quickly block the adsorption column, making the recovery process difficult. Moreover, many other interfering and undesired pollutants would interfere with the recovery process. For this reason, the recovery of polyphenols will be accomplished on a pretreated stream that is the concentrate of nanofiltration which is produced after the treatment of the raw wastewater by flocculation, photocatalysis and ultrafiltration. The concentrate of nanofiltration is rich enough of polyphenols to permit a suitable recovery from a technical and economical point of view.

2. Materials and methods

2.1 Packaging of wastewaters from olive mills

The samples of water were placed in 30 L bottles and were transported to the laboratory. The samples of OMWW were kept at -20°C for the later use. The research process developed in the laboratory for processing OMWWs is comprised of the steps described below.

2.2 Protocol processing of OMWW in laboratory pilot

The processes applied during the treatment of agro-food wastewaters (OMWW) and valuable compounds recovery are the following:

2.2.1 Sieving of OMWW

The OMWW were separated from solid particles by using a 300-micron sieve.

2.2.2 Clarification by coagulation-flocculation for removing particles

The coagulation helps to destabilize the suspended particles and facilitate their agglomeration. This method is characterized by injecting and dispersing chemicals. The flocculation aims to promote contact between the destabilized particles through slow mixing. These particles combine to form a flock which is removed by decantation. The water flocculation was performed by nitric acid at the temperature of 50°C and the initial pH of 5.2 was reduced to 3.0; followed the photocatalysis.

2.2.3 Photocatalysis

The heterogeneous photocatalysis is based on the interaction of the light and nanoparticles. Photocatalysis has been an innovative and promising technique for the purification of wastewater. The titanium dioxide (TiO_2) is the most of the common catalyst used nowadays due to its high performance, low cost, high photoactivity, low toxicity, chemical stability, insolubility and the resistance to photo-corrosion. The photocatalysis of clarified water stirred by a stirrer type Heidolph RZR 2014 was carried out by [16, 17]; on magnetic nanoparticle size of 79 nm coated with titanium oxide. The device is irradiated by a UV lamp VL-315 BLB 3x15W-385 nm Tube Power 90 W made in France for 4 h followed by the membrane treatment.

2.2.4 Ultrafiltration

The clarified OMWW was ultra-filtered on GM membranes, GK, GH and GE Type (TFM) tubular listed in **Table 1** with the cutoff between 100 and 200 kDa, and the recovering of the permeate. The ultrafiltration method is followed by nanofiltration.

2.2.5 Nanofiltration step

The permeate obtained by ultrafiltration is nano-filtered on DK and DL; spiral and tubular membranes type (TFM) listed in **Table 1** with the cutoff between 150

ID	Type of operation	Material	P _{max}	T _{max}	Pore size
JX	MF (microfiltration)	PVDF	12	T _{max}	300.00nm
JW	UF (ultrafiltration)	PVDF	12	50°C	n.d
GM	UF	TFM	16	50°C	2.00 nm
GK	UF	TFM	16	50°C	1.63 nm
GH	UF	TFM	16	50°C	0.90 nm
GE	UF	TFM	16	50°C	0.63nm
DL	NF(nanofiltration)	TFM	32	50°C	0.65 nm
DK	NF	TFM	32	50°C	0.50 nm
AK	RO (reverse osmosis)	TFPS	70	50°C	< 0.1 nm
SG	RO	TFPP	70	50°C	< 0.1 nm
SC	RO	TFPP	70	50°C	< 0.1 nm

PVDF: difluorure de polyvinyl, TFC or TFM: thin-film composite membranes, TFPP: talc filled polypropylene co-polymer, TFPS: thin-film polymer on silicon.

Table 1.
Characteristics of membrane modules used.

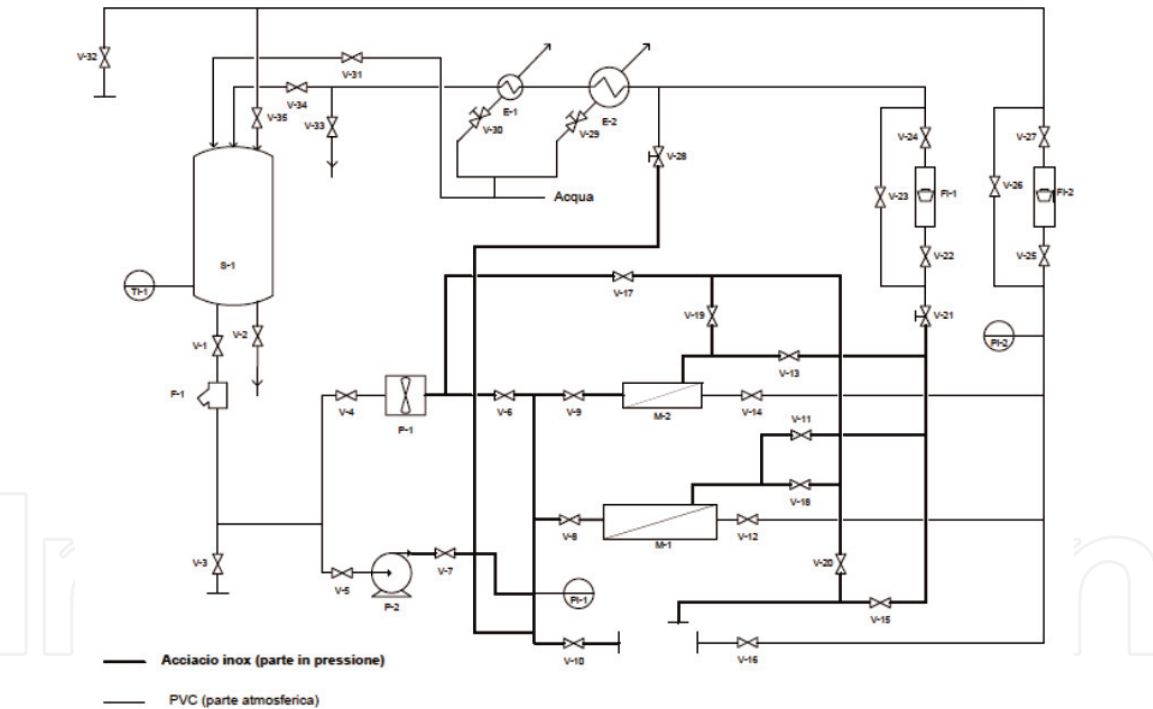


Figure 1.
Schematic of the pilot plant used.

and 400 Da, and at the maximum pressure of 16 Bar. Following this operation is obtained the rich fraction in polyphenols called nanofiltration concentrate. This concentrate is used in the adsorption/desorption tank for the separation of toxic compounds and the recovery of polyphenols of interest. If the operation is pursued we have the reverse osmosis which leads to the production of pure water. The membrane characteristics of this operation are recorded in **Table 1** and both **Figures 1** and **2** present the installation of the pilot plant used in the membrane treatment.



Figure 2.
 Photography of the pilot plant used (Ecosystem S. L Technologies).

2.3 Schematic description of the pilot plant

The pilot plant used is Ecosystem S. L Technologies and described as the following [18–21]:

S₀₁: Feed tank with the capacity: min 10 liters, max 100 liters where is introduced the water to be treated.

F₀₁: Cartridge filters of 50 μm to remove power remaining solids.

P₀₁: Volumetric pump.

P₀₂: Centrifuge pump.

M₀₁: Housing for medium size membrane modules, mod. 2540, area 2.51 m².

M₀₂: Housing for small size membrane modules, mod. 1812, area 0.52 m².

FI₀₁: Flow-meter concentrate stream.

FI₀₂: Flow-meter permeate stream.

E₀₁: concentrate heat exchanger (big).

E₀₂: concentrate heat exchanger (small).

V_{xx}: valves ($x = 1, 2, 3, \dots, 35$).

OMMW pre-treated feedstock was stored in a feed tank (FT1) of 100 L. The centrifugal (P1) and volumetric (P2) pumps to drive the wastewater stream over the spiral-wound membrane supplied by osmotic fitted in the housing M1, at a flow rate of 600 L/h. The active membrane area of each module was 2.51 m² [18–21].

The maximum one for the used membranes in this work that can be obtained constantly on this system, for the ultrafiltration (“UF”), the nanofiltration (“NF”) and the reverse osmosis (“RO”) type is reported in **Table 2**. The membranes are characterized when new by their pure water permeability value m_w , the average of the pore size D_p and the maximum operating pressure P_{max} . The membrane modules were used under the flux threshold conditions at least of 1000 operating hours. Each module exhibited reduced pure water permeability values compared to new ones. By acting on the regulation valves V_1 and V_2 , it was possible to set a desired operating pressure P_{ExT} over the membrane by maintaining a feed constant flow rate with an accuracy of 0.5 bar. The permeate and concentrate streams were cooled down to the feedstock temperature, mixed together and the feedstock composition was maintained constant during each experimental batch run. The temperature was

set at $20 \pm 1^\circ\text{C}$ for all experiments [18, 19, 22]. The pretreatment processes aim to reduce TSS and organic matter by measuring the COD. The results obtained by the authors [18, 19, 22] are shown in **Table 2** and are reported as a percentage of the reduction ($\Delta\%$). The adsorption step on polymeric resins is applied after the membrane treatment and obtaining the fraction of nanofiltration.

2.4 Characteristic and activation of FPX66 and MN202 resins

FPX66 and MN202 resins were provided courtesy of Rohm & Haas aromatic and Purolite Ltd., respectively. The physicochemical characteristics of these resins are summarized in **Table 3**. FPX66 and MN202 resins were activated by using sodium

Type	Characteristic of membrane modules [18, 19, 22]				
	Id	m_w [L/hm ² bar]	m_w [L/hm ² bar]	D_p [nm]	P_{max} [bar]
UF	Osmonics model GM	16.3	4.8	2.0	16
NF	Osmonics model DK	7.9	5.2	0.5	32
RO	Osmonics model SC	2.7	2.6	< 0.1	65
Stream	Pretreatment of OMWW raw materials [18, 19, 22]				
	COD		TSS		pH
	[g/L]	$\Delta\%$	[g/L]	$\Delta\%$	—
Raww OMWW	32.4	—	33.0	—	5.2
After flocculation	22.2	31.5	10.9	66.9	3.1
After centrifugation	19.2	13.5	8.4	22.9	—
After photocatalysis	16.5	14.1	5.2	38.1	—

Table 2.
Characteristics of the membrane and the pretreatment of OMWW.

Properties	FPX66	MN202
Physical form	White spherical beads	White spherical beads
Matrix	Macro-reticular aromatic polymer	Macroporous polystyrene cross-linked with divinylbenzene
Moisture holding capacity	60–80%	50–60%
Shipping weight	680 g/L	655–685 g/L
Specific gravity	1.015–1.025	1.04
Surface area ⁽²⁾	$\geq 700\text{ m}^2/\text{g}$	$825\text{ m}^2/\text{g}$
Porosity ⁽²⁾	$\geq 1.4\text{ cc/g}$	$1\text{--}1.1\text{ mL/g}$
Mean diameter	Harmonic mean size 0.600–0.750 mm	$535 \pm 85\text{ }\mu\text{m}$
Particle size	≤ 2.0	d50, meso and macropores: 600–900
• Uniformity coefficient ⁽¹⁾	<0.300 mm:3.0% max	D50, micropores: 15
• Fine content ⁽¹⁾	>1.180 mm:5.0% max	
• Coarse beads ⁽¹⁾		

Table 3.
Physicochemical characteristics of the resins FPX 66 and MN202.

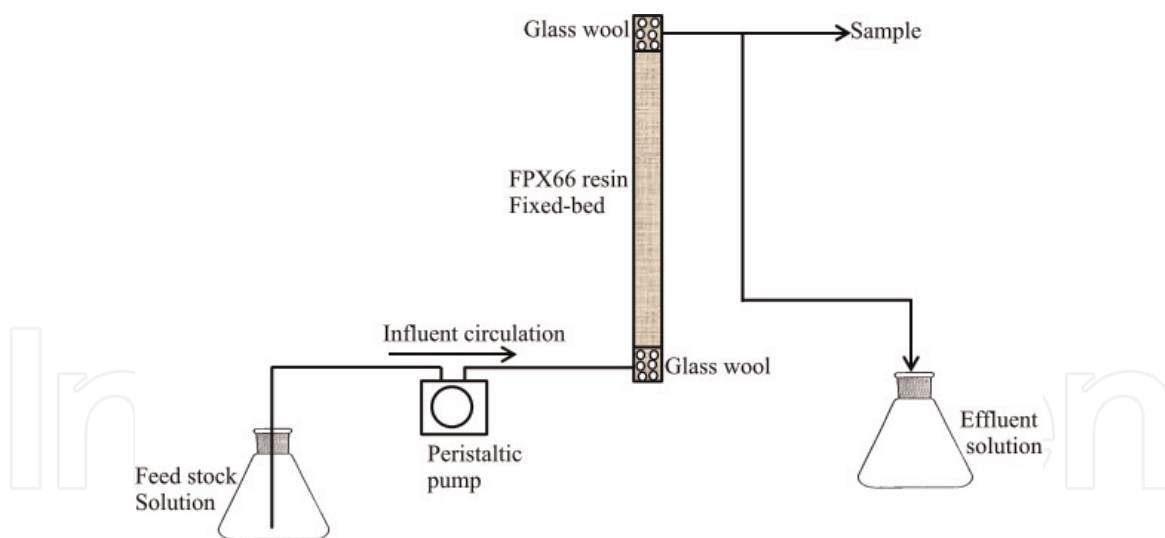


Figure 3.
 Schematic of the experimental setup in upward mode.

chlorite and washing with distilled water and then filtrating with a Buchner filter connected to a vacuum pump system. The filtrated resins were put into the beakers that already contained distilled water and the resulting solution was then left at constant stirring (70 rpm) for an hour. At the end of this procedure, the quantities of dissolved salts were evaluated through a digital conductivity meter. Since the results were not satisfactory, the new filtrations were made and the stirs were repeated, again for 60 minutes.

The solutions were again measured at the end and the decreases in salt concentrations were revealed. Finally, the treated resins were put into others beaker containing 96% ethylic alcohol, and then the contents of the beakers were stirred (120 rpm) for an hour. After this procedure, the resins were filtrated and conserved in a distilled water environment ready for use.

2.5 Column adsorption and desorption experiments

Lab-scale packed bed column experiments were carried out to evaluate the performance of the resin for the adsorption of phenolic compounds. In a typical procedure, the fixed-bed columns were made of Pyrex glass tubes of 1 or 2 cm inner diameter with 9.5 and 19.5 cm height respectively. The model column was packed with the adsorbent between glass wool and supported by inert glass beads as shown in **Figure 3**.

The column performance adsorption onto resin was studied at different phenol concentrations of 200, 400 and 600 mg/L, bed height 9.5 and 19.5 cm and flow rate between 0.8–4.0 mL/min. The bed diameters and depths took were 10.0 and 19.5 cm (resin mass of 5.07 g), 2.0 and 19.5 cm (resin mass of 41.6 g), respectively. The influent of phenol solution was pumped in an upward mode with a peristaltic pump in order to avoid channeling inside the column.

2.5.1 Performance indicators in a fixed-bed column

The breakthrough curves showed the loading behaviour of phenol, tyrosol and hydroxytyrosol to be removed in a fixed bed. It is expressed in normalized concentration defined as the ratio of effluent solute concentration to inlet (feed) solute concentration (C_{out}/C_{in}), as a function of time or volume of effluent for a given bed height [23].

Effluent volume (V_{eff}) can be calculated by the following relationship:

$$V_{\text{eff}} = Q \cdot t_{\text{total}} \quad (1)$$

where Q and t_{total} are the volumetric flow rate (mL/min) and the total flow time (min). The adsorption performance for a given bed mass is directly related to the number of bed volumes (BV) processed before the breakthrough point is reached [24]. The number of bed volumes treated before a breakthrough can be calculated as follows:

$$BV = \frac{\text{Volume of water treated at breakthrough point (L)}}{\text{Volume of adsorbent (L)}} \quad (2)$$

The rate for saturating the adsorbent during adsorption run was used to determine the regularity at which the adsorbent was replaced or regenerated. The adsorption exhaustion rate (AER), where low AER values imply the good performance of the bed was given by [23, 25] Eq. (3):

$$AER = \frac{\text{mass of adsorbent (m, (g))}}{\text{Volume of water treated (L)}} \quad (3)$$

The area under the breakthrough curve (A) calculated by integrating the plot of adsorbed concentration (C_{ad} ; mg/L) versus t (min) and used to find the total adsorbed phenol or tyrosol quantity (maximum column capacity). The total adsorbed phenol or tyrosol quantity (q_{total} ; mg) in the column for a given feed concentration and the flow rate was calculated as the following:

$$q_{\text{total}} = \frac{QA}{1000} = \frac{Q}{1000} \int_{t=0}^{t=t_{\text{total}}} c_{\text{ad}} dt \quad (4)$$

The total amount of phenol or tyrosol in feed sent to column (m_{total} ; mg) is calculated by:

$$m_{\text{total}} = \frac{C_{\text{in}} Q \cdot t_{\text{total}}}{1000} \quad (5)$$

Equilibrium phenol/tyrosol uptake (q_{eq} ; mg/g) (or the maximum capacity of the column) in the column is defined as the total of solute adsorbed (q_{total}) per g of adsorbent (X ; g) at the end of total flow time, that is:

$$q_{\text{eq}} = \frac{q_{\text{total}}}{X} \quad (6)$$

The column performance (Total removal percentage of solute) can be defined as the ratio of the total adsorbed quantity of phenol/tyrosol (q_{total}) to the total amount sent to the column as follows:

$$\text{Column performance (\%)} = \frac{q_{\text{total}}}{m_{\text{total}}} \times 100 \quad (7)$$

Unadsorbed phenol/tyrosol concentration at equilibrium in the column (C_{eq} ; mg/L) can be defined by the following relationship:

$$C_{\text{eq}} = \frac{m_{\text{total}} - q_{\text{total}}}{V_{\text{eff}}} \times 1000 \quad (8)$$

In respect to the breakthrough separation of phenol, tyrosol and HO-tyrosol in binary and in OMWW NF concentrate:

A. Tyrosol solution with 100% purity is represented by Time (h) in which the outlet contains the only tyrosol since its breakpoint (B.T = Breakthrough time) as:

$$\Delta V_{100}(\text{mL}) = Q [\text{Time}_{(100\%)} - \text{Time}_{(\text{B.T})}] \quad (9)$$

B. Tyrosol solution with 90% purity is represented by Time (h) in which the outlet contains the only tyrosol at 90% and phenol at 10% since its breakpoint (B.T = Breakthrough time) as:

$$\Delta V_{90}(\text{mL}) = Q [\text{Time}_{(90\%)} - \text{Time}_{(\text{B.T})}] \quad (10)$$

C. In multi-component system OMWW NF concentrate, polyphenol solution with 100% purity (tyrosol and hydroxytyrosol) is represented by latest time (h) at which the outlet stream contains the target polyphenols of this study, that is tyrosol and hydroxytyrosol, at 100% purity towards phenol since their breakpoint (B.T = Breakthrough time) as:

$$\Delta V_{100}^*(\text{mL}) = Q [\text{Time}_{(100\%)} - \text{Time}_{(\text{B.T})}] \quad (11)$$

D. Tyrosol+ Hydroxytyrosol solution with 90% purity is represented by Time (h) in which the outlet contains only tyrosol+ hydroxytyrosol at 90% and phenol at 10% since its breakpoint (B.T = Breakthrough time) as:

$$\Delta V_{90}^*(\text{mL}) = Q [\text{Time}_{(90\%)} - \text{Time}_{(\text{B.T})}] \quad (12)$$

2.5.2 Breakthrough model studies

2.5.2.1 Thomas model

The Thomas model is widely used in column performance modeling. Its derivation assumes Langmuir kinetics of adsorption-desorption and no axial dispersion. The expression for the Thomas model for adsorption column is given by [26]:

$$C^* = \frac{C_{\text{out}}}{C_{\text{in}}} = \frac{1}{1 + \exp \left[\left(\frac{k_{\text{Th}} q_e X}{Q} \right) - k_{\text{Th}} C_{\text{in}} t \right]} \quad (13)$$

where k_{Th} (mL/min/mg) a Thomas constant, q_e (mg/g) the predicted adsorption capacity, m mass of adsorbent (g), Q influent flow rate (mL/min), C_{in} the initial concentration (mg/L), and C_{out} effluent concentration (mg/L). The linearization of the Thomas model was expressed in Eq. (14):

$$\text{TM} = \ln(C^* - 1) = \frac{k_{\text{Th}} q_e X}{Q} - k_{\text{Th}} C_{\text{in}} t \quad (14)$$

2.5.2.2 Yoon-Nelson (YN) model

Yoon-Nelson model as other models did not require data about the characteristics of the system such as well as the type of adsorbent and physical properties of adsorption bed.

The YN was expressed as follows [27]:

$$\frac{C_{out}}{C_{in} - C_{out}} = \exp(k_{YN}t - \tau k_{YN}) \quad (15)$$

where k_{YN} (L/min) the rate constant and τ (min) the time required for 50% of adsorbate breakthrough. The linear form of YN model was expressed as follows:

$$YN = \ln \frac{C_{out}}{C_{in} - C_{out}} = k_{YN}t - \tau k_{YN} \quad (16)$$

2.5.2.3 Adams-Bohart (AB) model

Adams-Bohart model was based on the assumption that the rate of adsorption was proportional to the concentration of adsorbed species and the residual capacity of adsorbent. The AB model was used to describe the initial part of the breakthrough curve and expressed as [24]:

$$C^* = \frac{C_{out}}{C_{in}} = \exp\left(k_{AB}C_{in}t - k_{AB}N_0 \frac{z}{U_0}\right) \quad (17)$$

Where k_{AB} (l/min.mg) is rate constant of Adams-Bohart model, z (cm) is the bed depth, N_0 (mg/L) is maximum ion adsorption capacity per unit volume of the adsorbent column, and U_0 (cm/min) is the linear velocity of influent solution. The linear form of Adams-Bohart model is expressed as follows:

$$ABM = \ln C^* = k_{AB}C_{in}t - k_{AB}N_0 \frac{z}{U_0} \quad (18)$$

2.6 Characterization techniques

2.6.1 Porosity and microporosity resins

2.6.1.1 Mercury porosimetry

Penetration of a liquid in a capillary is related to the shape and dimensions of the capillary, and the surface tension of mercury and the pressure that is exerted on the latter. The relationship between the pressure and the pore radius in the case of a cylindrical pore is given by the following equation:

$$p.r = 2\gamma \cos \theta \quad (19)$$

where r : is the pore radius.

γ : mercury surface tension and equals to 480 mN.m^{-2} . (Data Carlo Erba).

θ : contact angle equal to 141.3 degrees (data Carlo Erba).

The measuring instrument used is the automatic mercury porosimetry 2000 Carlo Erba, it gives a distribution based pore volume and the cumulative volume per cent.

2.6.1.2 Measurement of micropores by t -plot method (thickness plot)

This method is used to estimate the volume and the surface of the micropores, or to characterize the material from the point of view of their porosity. The data

provided is the surface area of meso and macropores, and the volume of micropores. It enables the determination of the specific surface area of the micropores when coupled with the BET method. The accepted parameters for characterizing materials according to the diameter (d in nm) pores are: micropores (d < 2 nm); mesopores (2 < d < 50) macropores (50 < d < 7500) and megapores (7500 nm < d).

The calculation method is based on the layout of the volume of gas adsorbed as a function of the thickness of the monomolecular film of the same gas. This diagram called thickness is subsequently used to evaluate quantitatively and qualitatively the porosity of the adsorbent. The film thickness is calculated by either equation Halsey Eq. (20) that of Harkins and Jura Eq. (21) [28].

$$t = \left(\frac{13.99}{\log \frac{P_o}{P_e} + 0.034} \right)^{1/2} \quad (20)$$

$$t = 3.54 \left(\frac{5}{2.303 * \log \frac{P_o}{P_e} + 0.034} \right)^{1/3} \quad (21)$$

By plotting the adsorbed volume according to the calculated thickness of the film, the intercept (Y) of this curve (t-plot) is converted to the volume of gas to liquid volume to provide micropores. The slope α of the linear section of the graph used to calculate the surface area of the mesopores and macropores. The corresponding formulas are given the following:

$$\text{Micropores Volume} = (0.001547) * Y \quad (22)$$

$$\text{Mesopores specific area} = 1547 * \alpha \quad (23)$$

The calculations also used to obtain the surface area A of the micropores as follows:

$$A = \text{BET specific area} - \text{Specific area of mesopores} \quad (24)$$

The shapes of the curves and hysteresis provide information on the porosity of the material studied according to the classification proposed by isothermal [29] and modified by International Union of Pure and Applied Chemistry (IUPAC) [30].

2.6.2 Determination of point of zero charge (PZC)

The points of zero charge of FPX66 and MN202 resins were determined [31]. In different flasks, 50 mL of NaNO₃ 0.1 mol/L was introduced and the pH of the solution was adjusted by using 1 mol/L NaOH or HCl to obtain a denoted pH_i value between 2 and 12. One gram of activated resin was then introduced in each flasks, covered and allowed to rest for 48 hours during which they were manually stirred. At the end of the operation, the pH of the solution (pH_f) was recorded. pH_{pzc} were derived from the curve $\Delta\text{pH} = \text{pH}_i - \text{pH}_f = f(\text{pH}_i)$ as the intercept of the abscissa for resins.

2.6.3 The specific surface area by the BET method

The determination of the recovery capacity by a mono-molecular layer of adsorbate (V_m) allows for the calculation of the specific surface. The number (V_m)

was calculated from the adsorption isotherm, mainly by the BET method depends on the surface, temperature and pressure (STP) and the form of the following linear transform:

$$A = \frac{P_e}{V_a(P_o - P_e)} = \frac{C - 1}{V_m C} \frac{P_e}{P_o} + \frac{1}{V_m C} \quad (25)$$

where V_m was the volume of a monolayer,

V_a = volume adsorbed at a relative pressure P_e/P_o ;

P_e = sample equilibrium pressure,

P_o = saturation vapor pressure of the gas to the temperature of the experiment,

C = relative constant to the enthalpy of adsorption.

The route of $A = f(P_e/P_o)$ is a line of a slope $(C - 1)/V_m C$, and intercepts origin at $1/V_m C$. In practice, this line was checked only in a limited area of relative pressure ($0.05 < P_e/P_o < 0.2$) and in many cases, it is always $C \gg 1$. The BET specific surface area (m^2/g) was then determined from the following expression:

$$S_{BET} = \frac{V_m \cdot N \cdot A_m}{M_v} = V_m \cdot A_m \cdot N \cdot 10^{-20} \text{ (m}^2\text{/g)} \quad (26)$$

where N = is Avogadro constant (6.02×10^{23}),

M_v = Molecular volume per gram ($22,414 \text{ cm}^3$),

A_m = area occupied by each molecule of adsorbate (0.162 nm^2 for N_2).

2.6.4 Analysis of phenolic compounds by HPLC

High-pressure liquid chromatography (HPLC) is a technique to identify compounds within a sample by measuring the retention time through a separation column transported by a proper bulk stream. The use of high pressure permits to fasten the separation and obtain the results quicker. The measurement is done by a mass spectrometer at the exit of the separation column and is capable to measure a peak in terms of mAU, strictly connected to the concentration of the compound.

In this work, a C18 column was used. The bulk stream is composed of an aqueous solution of 1% of acetic acid. At the start of each experimental run and afterwards at regular time intervals, samples were withdrawn every 15 min, filtered through a cellulose acetate membrane filter (0.20 mm, Schleicher & Schuell) and analyzed. 25 μ L of the sample was injected into the HPLC system. The temperature of the column was 20°C and the flow-rate was 1 mL/min. The mobile phase: 0.5% acetic acid volume ("A") and acetic nitrile ("B"). Elution was performed under conditions:

- At the start of 2 min of the run with 100% of A.
- From 2 to 60 min 40% of A and 60% of B.

Polyphenols were detected by a UV detector (280 nm). Beforehand, the retention times of the polyphenolic compounds of interest were measured using single phenol, tyrosol and OH-tyrosol standard solutions ranging from a concentration of 100–600 mg/L. The chromatographic parameters, described in the following in **Table 4** [32, 33].

The quantification was based on the size of the chromatogram peaks and achieving a standard range is developed for each of the standards polyphenols.

Parameters	Details
Mediterranea sea column Serial number: NF-21905	C18, thickness: 5µm, length 25 cm Diameter: 0.46 mm
Pressure	150 bars
Temperature	20°C
Flow rate	1.0 mL/min
Eluant	Acetonitrile + acetic acid 0.5%
Injection volume	20 µL
Wavelength	280 nm

Table 4.
HPLC parameters for the determination of polyphenols.

3. Fixed bed studies

3.1 Effect of initial phenol concentration

The sorption breakthrough curves obtained at inlet phenol concentrations of 200, 400 and 600 mg/L at 0.106 L/h flow rate are given in **Figure 4**. A decreasing inlet concentration gave a later breakthrough curve as displayed in **Figure 4**. The treated volume was greatest at the lowest inlet concentration due to a lower concentration gradient caused a slower transport and the decreasing in diffusion coefficient or decreasing in mass transfer coefficient. The breakpoint time decreased with increasing inlet phenol concentration as the binding sites became more quickly saturated in the system. The breakthrough concentration ($C_t/C_o = 0.03$) occurred after 30 hours (3000 mL of effluent) i.e. 200 mg/L phenol inlet concentration. It appeared after 17 hours and 15,5 hours corresponding to 1700 mL and 1550 mL of inlet concentration of phenol 400 and 600 mg/L, respectively.

3.2 Effect of the flow rate

The effect on flow rate for the adsorption of phenol at flow rates 0.8; 2.0 and 4.0 mL/min at an influent concentration of 600 mg/L and bed height 19.5 cm displayed in **Figure 5**. It was clearly observed that a rapid uptake was noticed in the initial stages of adsorption and decreases thereafter and finally reaches saturation. The increase in flow rate, the breakthrough curves become steeper and reach the breakpoint quickly. This probe displayed a well-defined of the residence time of the solute in the column, which was not long enough for adsorption equilibrium to be reached at a high flow rate. So at the high flow rate, the phenol solution left the column before equilibrium occurs. Furthermore, a fixed saturation capacity of bed based on the same driving force gave rise to a shorter time for saturation at a higher flow rate [8, 34, 35].

3.3 Effect of bed height

The breakthrough curves for the adsorption of phenol on macro-aromatic resin FPX66 at various bed heights by fixing the influent concentration at 600 mg/L and flow rate at 2 mL/min are given in **Figure 5**. The results indicated that the through-put volume of phenol solution increased with increasing bed height, due to the

availability of more sorption sites due to the increase in the total surface for adsorption [34]. The equilibrium capacity decreases with the increase of the bed height. In a fixed bed method the probability of contact between the adsorbate and the adsorbent is less when compared to the batch mode, which results in lesser equilibrium sorption capacity in column mode.

3.4 Dynamic adsorption models

3.4.1 Thomas model

The adsorption data were applied to the Thomas model and the results are presented in Table 5.

Table 5 shows that the Thomas constant (k_{Th}) as the equilibrium capacity $q_{0(Th)}$ increases with the increase of the phenol concentration, the bed height increases with the decrease of the flow rate. A negligible difference was observed between experimental and calculated values of the bed capacity $q_{0(Th)}$ obtained at all inlet phenol concentrations studied although the deviations of experimental data from predicted values were evident at 2.0 and 4.0 mL/min flow rates. Thomas model gives a good correlation with the experimental data at flow rates, bed heights for all

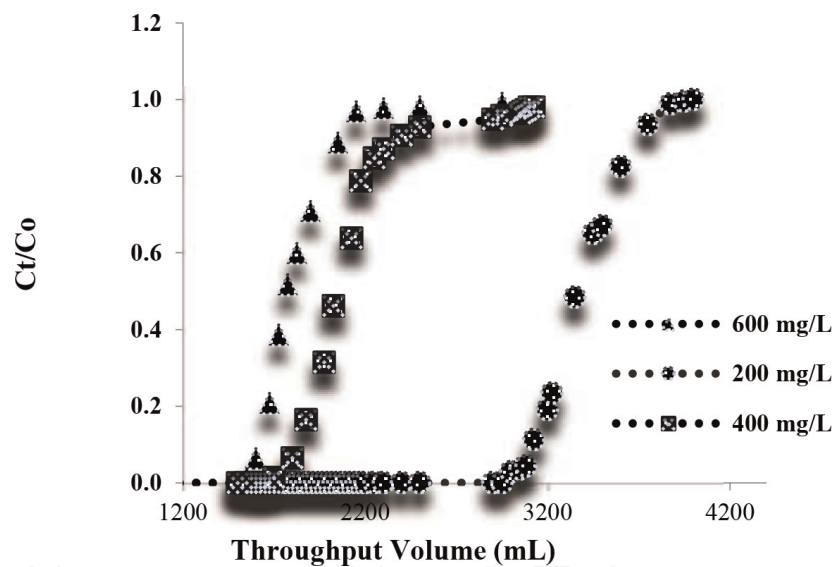


Figure 4. Throughput volume and breakthrough for phenol at inlet concentrations.

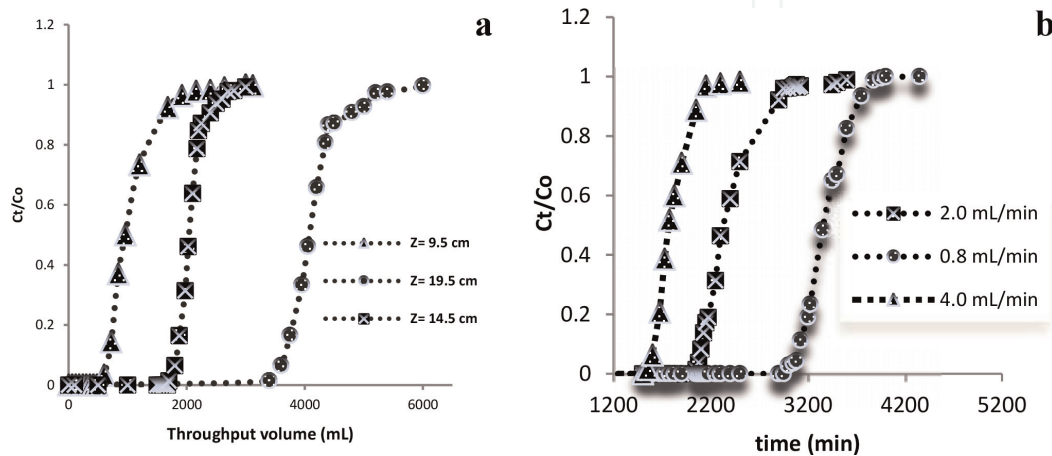


Figure 5. Effect of bed height (a) and flow rate (b) for the removal of phenol on FPX66 column.

Parameters		Experimental conditions				
Feed stock C_0 (mg/L)	200	400	600	400	400	400
Flow rate Q (mL/min)	2.0	2.0	2.0	4.0	2.0	2.0
Bed height Z (cm)	19.5	19.5	19.5	19.5	9.5	14.5
Mass of sorbent X (g)	41.6	41.6	41.6	41.6	20.8	30.9
Mass sorbate X (mg)	1372.84	1740.50	2204	1603.90	814.23	1336.92
q_0 (exp) (mg/g)	31.40	41.84	52.98	48.55	39.15	40.26
Thomas parameters at different conditions using linear regression analysis						
k_T (mL/min/mg) $\times 10^{-5}$	2.08	2.13	3.21	3.12	2.7	2.43
q_0 (Th) (mg/g)	32.48	42.44	51.34	48.35	40.16	43.14
R^2	0.984	0.910	0.961	0.915	0.914	0.918
Sd	0.18	0.10	0.27	0.03	0.16	0.48
Yoon-Nelson parameters at different conditions using linear regression analysis						
q_0 (YN) (mg/g)	29.64	36.15	41.26	48.30	48.61	37.64
K (YN) (L/min) $\times 10^{-2}$	1.12	1.14	1.93	1.25	1.07	0.85
τ (min)	3082	1879	1430	1256	1264	1454
R^2	0.959	0.918	0.961	0.15	0.914	0.966
Sd	0.29	0.94	1.95	0.04	1.57	0.43

Table 5.
Thomas and Yoon-Nelson kinetic model for phenol onto FPX66 in a fixed bed.

inlet phenol concentrations. Thomas model is suitable for adsorption processes where the external and internal diffusions will not be the limiting step [34, 36].

3.4.2 Yoon-Nelson model

Table 5 showed the rate of constant k_{YN} of Yoon-Nelson increased with increasing phenol concentration. This was due to the fact that the increase in initial phenol from 200 to 600 mg/L. This displayed an increase in the competition between phenol molecules for the adsorption sites, which ultimately results in increased uptake rate. The rate constant increased with increasing the flow rate and decreased with an increase in bed height. At high flow rate, the number of phenol molecules passing through an adsorbent was more which increased the rate. The time required for 50% breakthrough τ decreases with increasing as the phenol concentration, flow rate and bed height.

The adsorption capacities calculated based on Thomas and Yoon-Nelson models are in good agreement with the observed value with high R^2 values and very low error analysis ($0.03 \leq Sd \leq 1.95$). Both models describe the behaviour of phenol onto FPX66 resin column. The obtained results are in agreement with other authors [34, 36, 37].

3.4.3 Adsorption of OMWW NF concentrate by FPX66 resin

In order to determine the adsorption effectiveness in a more complex and realistic scenario, the FPX66 resin in fixed mode was exposed to an OMWW NF concentrated containing all polyphenols from the membrane of nanofiltration plant selected for this work [21, 22, 38]. The influent flow rate was kept at a constant flow

rate of 2 mL/min whereas the bed height, the diameter of the column and resin particle size were $Z = 3.8$ cm, $D = 4$ cm, $0.600 \leq d \leq 0.750$ mm) at ambient temperature, respectively.

A considerable reduction in breakthrough time was observed for tyrosol i.e. 12; 11.5 and 6.5 hours respectively in single, binary and multiple component systems. Although the increase of breakthrough time was observed for the phenol during 17; 18 and 22.5 hours respectively proved that the selectivity was observed for phenol than other polyphenols by the FPX66 resin.

This could be attributed to competition between adsorbates for the same sites and adsorbates include benzoic acids and its derivatives (gentisic, vanillic, gallic, syringic acids), cinnamic acids and derivatives such as caffeic, ferulic, sinapic acids, and phenolic alcohols, secoiridoides aglycones (oleuropein, ligstroside), flavonols, flavones and fignans etc. coexisting frequently in OMWW (**Figure 6**) and more in NF concentrate [18, 39, 40]. The macro-reticular aromatic resin pore adsorption sites could be blocked by the polyphenol molecules.

The overall outlet capacities estimated for the tyrosol and the hydroxytyrosol were only slightly enhanced plausibly indicating a combination of pore blockage and unique interactions with the FPX66 surface. Phenol ($pK_a = 9.95$) has a net neutral charge, so that means binding onto FPX66 is probably to be attributed to several types of molecular interactions, including hydrophobic interaction, hydrogen bonding, ionic attraction and complex formation [41]. Azonova and Hradil [42] found that hydrophobic interaction was the binding mechanism for adsorption by the hypercrosslinked Amberlite XAD-4. In addition, Maity et al. [43] showed that the degrees of adsorption for phenols, alcohols and aromatic amines increased with the strength of the hydrogen bond between the organic chemicals and the resin. Juang and Shiau [44] found that adsorption of phenol and chlorophenol by the macroporous Amberlite XAD resins was affected by the resin's hydrophobicity, the number of active sites and pore size distribution. By comparing the adsorption of five organic chemicals, Weber and Van Vliet [45] concluded that hydrophobic interaction played a key role in the adsorption of macroporous Amberlite XAD resins. In addition, the swelling of resin-like, in this case, increases the volume of the polymer phase and, thus, the absorption capacities of organic chemicals and it is

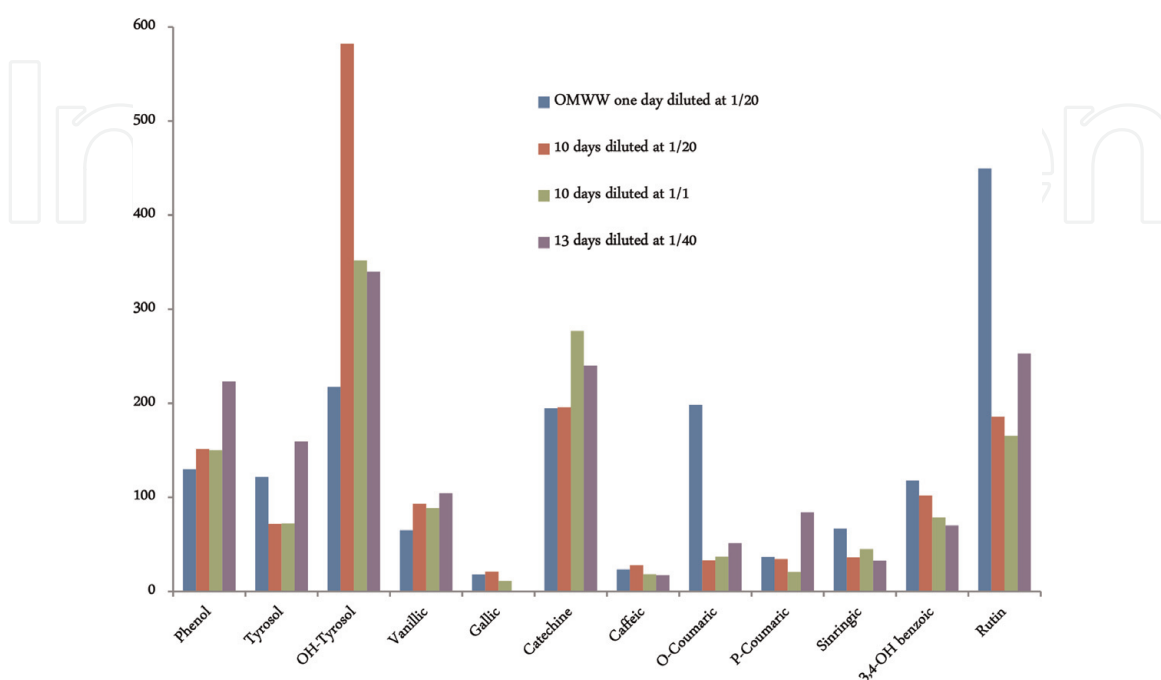


Figure 6.

Profile of the phenolic compounds identified in nanofiltration fraction of OMWW.

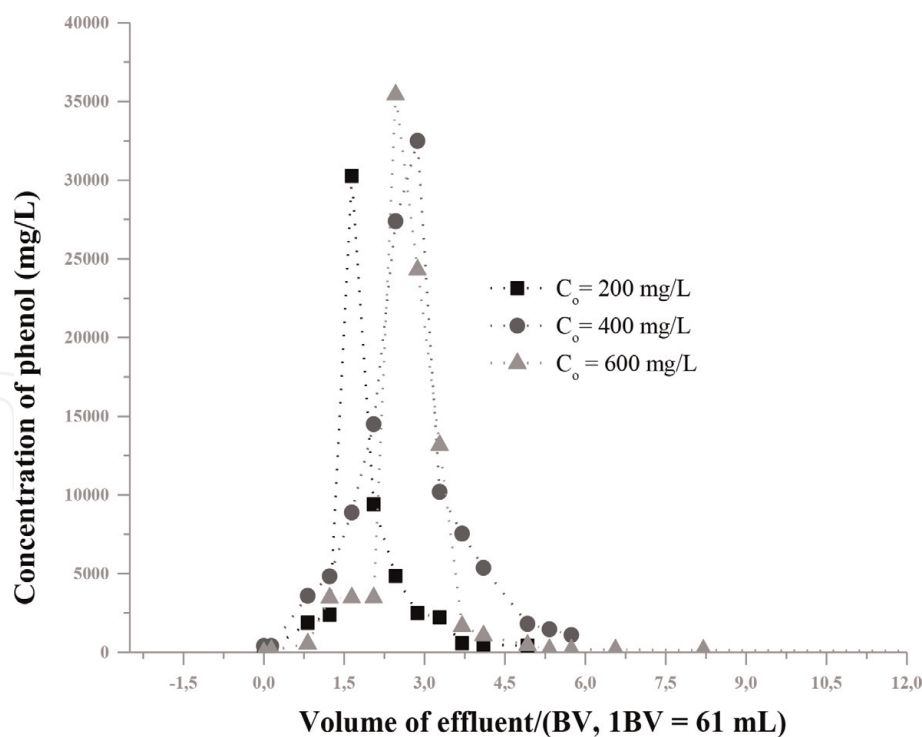


Figure 7.
 Dynamic desorption curves of phenol concentrations on FPX66 resin.

probably affected by hydrogen bonding of polar organic chemicals and the macroporous resins, such as Amberlite XAD-8 [43].

3.5 Dynamic adsorption/desorption

After the dynamic adsorption experiments, a 50% (v/v) EtOH solution at a flow rate of 0.1 L/h was used to purge the resin column. Desorption results are displayed in **Figure 7** for different inlet phenol concentrations of 200, 400 and 600 mg/L. About 3.0; 5.0 and 6.0-bed volumes of 50% (v/v) EtOH aqueous solution were used to regenerate the FPX66 resin column, for initial phenol concentrations of 200, 400 and 600 mg/L respectively. The desorption capacities of phenol from FPX66 resin were calculated to be 31.86, 37.06 and 48.00 mg/g at initial phenol concentrations of 200, 400 and 600 mg/L, respectively, which agrees well with the dynamic adsorption capacities of phenol with three inlet columns. This is also in agreement with the results obtained by Li *et al.* [46].

4. Conclusions

The study, we can conclude that FPX66 resin is an effective adsorbent for phenol removal from aqueous solutions.

From batch investigations, the effect of contact time for phenol removal by the FPX66 resin showed rapid adsorption of phenol in the first 30 min. The equilibrium data were fitted by Langmuir, Freundlich, Temkin and Dubinin-Radushkevich isotherms with good correlation coefficient R^2 . The adsorption kinetics followed the pseudo-second-order model with a maximum capacity of 28.44 mg/g and obeyed the intra-particle diffusion with high R^2 (>0.999). Higher desorption efficiency was obtained after 20 min of shaking time and the percentage of desorption decreased with the increase in the initial concentration of phenol.

From the fixed bed investigations, as the flow rate increased, the breakthrough curve became steeper. The breakpoint time was obtained earlier at a high flow rate and effluent phenol concentration ratio increased more rapidly. For lower bed height, the effluent phenol concentration ratio increased more rapidly than for higher bed height. For larger initial phenol concentration, steeper breakthrough curves were obtained and breakpoint time was achieved sooner. The column experimental data were fitted well to the Thomas and Yoon-Nelson models. Coming to the end, we can draw a conclusion that, the use of resin column could be completely regenerated by a 50% (v/v) ethanol aqueous solution.

Acknowledgements

The authors express the sincere thanks to the European Commission for the Fellowship ‘Erasmus Mundus ACP’ offered and the Department of Chemical Materials Environmental Engineering of the University of Rome “La Sapienza” for their hospitality and access to scientific instrumentation.

Conflict of interest

The authors declare that there is no conflict of interests.

Acronyms and abbreviations

OMWW	olive mill wastewater
FPX66	macro-reticular aromatic polymer
MN202	macroporous polystyrene cross-linked with divinylbenzene
EPA	Environmental Protection Agency
EU	European Union
GAC	granular activated carbon
MF	microfiltration
UF	ultrafiltration
NF	nanofiltration
RO	reverse osmosis
PVDF	difluorure de polyvinyl
TFC or TFM	thin-film composite membranes
TFPP	talc filled polypropylene co-polymer
TFPS	thin film polymer on silicon
BV	bed volumes
BT	breakthrough
AER	adsorption exhaustion rate
IUPAC	International Union of Pure and Applied Chemistry
PZC	point of zero charge
STP	surface, temperature and pressure
HPLC	high pressure liquid chromatography

Nomenclature

A	area under the breakthrough curve obtained by integrating (C_{ad}) versus t (mg min/L)
AER	adsorption exhaustion rate (—)

BV	bed volumes (mL)
C^*	normalized concentration (–)
C	constant that gives an idea about the thickness of the boundary layer (mg/g)
C_{ad} ($C_{ad} = C_o - C_t$)	adsorbed phenol concentration (mg/L)
C_d	concentration in the desorption solution (mg/L)
C_e	equilibrium concentration of phenol (mg/L)
C_{max}	highest initial concentration in solution (mg/L)
C_o	initial concentration (mg/L)
C_t	effluent concentration (mg/L)
D	desorption ratio of the resin (%)
k_{Th}	Thomas rate constant (L/min/mg)
k_{YN}	Yoon-Nelson rate constant (1/min)
m	initial mass of resin in batch mode (g)
m_{total}	total amount of phenol in the feeding sent to the column (mg)
Q	volumetric flow rate (mL/min)
$q_{0(Th)}$	maximum Thomas adsorption capacity (mg/g)
$q_{0(cal)}$	adsorption capacity calculated using three models (mg/g)
q_t, q_e	amounts of adsorbed at time t and at equilibrium (mg/g)
R	gas constant (J/mol/K)
R^2	determination coefficient associated with data fitting (–)
t, t_{total}	time and total flow time (min)
T	temperature (K)
V	volume of solution (L)
V_d	volume of desorption solution (L)
V_{eff}	effluent volume (mL)
X	amount of adsorbent in the column (g)
Z	bed height column or upward vertical axial distance inside the fixed bed (cm)
ε	void fraction in the bed (–)
ρ_a	density of the adsorbent material (g/L)
τ	time required for 50% of adsorbate breakthrough (min)

Author details

Jacques Romain Njimou^{1,2*}, Fridolin Kouatchie Njeutcha³, Emmanuel Njungab^{4,5}, André Talla^{3,4} and Nkeng George Elambo³

1 Laboratory of Analytical Chemistry, Faculty of Sciences, University of Yaoundé I, Yaoundé, Cameroon

2 School of Chemical Engineering and Mineral Industries, University of Ngaoundere, Ngaoundere, Cameroon


3 Research Center, National Advanced School of Public Works, Yaounde, Cameroon

4 Energy, Water and Environment Laboratory, National Advanced School of Engineering, University of Yaounde, Yaounde, Cameroon

5 Institut Universitaire des Sciences des Technologies et de l'éthique de Mendong, Yaounde, Cameroon

*Address all correspondence to: njimoujacques@gmail.com

IntechOpen

© 2019 The Author(s). Licensee IntechOpen. This chapter is distributed under the terms of the Creative Commons Attribution License (<http://creativecommons.org/licenses/by/3.0>), which permits unrestricted use, distribution, and reproduction in any medium, provided the original work is properly cited. 

References

- [1] Hill GA, Robinson CW. Substrate inhibition kinetics: Phenol degradation by *Pseudomonas putida*. Biotechnology and Bioengineering. 1975;1599-1615
- [2] Adhoum N, Monser L. Decolourization and removal of phenolic compounds from olive mill wastewater by electrocoagulation. Chemical Engineering and Processing Process Intensification. 2004;43(10): 1281-1287. DOI: 10.1016/j.cep.2003.12.001
- [3] Balice V, Cera O. Acidic phenolic fraction of the juice of olives determined by gas chromatographic method. Grasas y Aceites. 1984;178-180
- [4] Lafka T-I, Lazou AE, Sinanoglou VJ, Lazos ES. Phenolic and antioxidant potential of olive oil mill wastes. Food Chemistry. 2011;125(1):92-98. DOI: 10.1016/j.foodchem.2010.08.041
- [5] Li A, Zhang Q, Zhang G, Chen J, Fei Z, Liu F. Adsorption of phenolic compounds from aqueous solutions by a water-compatible hypercrosslinked polymeric adsorbent. Chemosphere. 2002;47(9):981-989. DOI: 10.1016/S0045-6535(01)00222-3
- [6] De Marco E, Savarese M, Paduano A, Sacchi R. Characterization and fractionation of phenolic compounds extracted from olive oil mill wastewaters. Food Chemistry. 2007; 104(2):858-867. DOI: 10.1016/j.foodchem.2006.10.005
- [7] Busca G, Berardinelli S, Resini C, Arrighi L. Technologies for the removal of phenol from fluid streams: A short review of recent developments. Journal of Hazardous Materials. 2008;160(2-3): 265-288. DOI: 10.1016/j.jhazmat.2008.03.045
- [8] Abdelkreem M. Adsorption of phenol from industrial wastewater using olive mill waste. In: 4th International Conference on Environmental Science and Development (ICESD 2013). Vol. 5. 2013. pp. 349-357. DOI: 10.1016/j.apcbee.2013.05.060
- [9] Ahmaruzzaman M, Sharma DK. Adsorption of phenols from wastewater. Journal of Colloid and Interface Science. 2005;287(1):14-24. DOI: 10.1016/j.jcis.2005.01.075
- [10] Anisuzzaman SM, Bono A, Krishnaiah D, Tan YZ. A study on dynamic simulation of phenol adsorption in activated carbon packed bed column. Journal of King Saud University-Engineering Sciences. DOI: 10.1016/j.jksues.2014.01.001
- [11] Lin S-H, Juang R-S. Adsorption of phenol and its derivatives from water using synthetic resins and low-cost natural adsorbents: A review. Journal of Environmental Management. 2009; 90(3):1336-1349. DOI: 10.1016/j.jenvman.2008.09.003
- [12] Richard D, Delgado Núñez M, Schweich D. Adsorption of complex phenolic compounds on active charcoal: Breakthrough curves. Chemical Engineering Journal. 2010; 158(2):213-219. DOI: 10.1016/j.cej.2009.12.044
- [13] Huang J, Wu X, Zha H, Yuan B, Deng SA. Hypercrosslinked poly (styrene-co-divinylbenzene) PS resin as a specific polymeric adsorbent for adsorption of 2-naphthol from aqueous solutions. Chemical Engineering Journal. 2013;218(0):267-275. DOI: 10.1016/j.cej.2012.12.032
- [14] Li H, Xu M, Shi Z, He B. Isotherm analysis of phenol adsorption on polymeric adsorbents from nonaqueous solution. Journal of Colloid and Interface Science. 2004;271(1):47-54. DOI: 10.1016/j.jcis.2003.10.026

- [15] Vázquez G, Alonso R, Freire S, González-Álvarez J, Antorrena G. Uptake of phenol from aqueous solutions by adsorption in a *Pinus pinaster* bark packed bed. *Journal of Hazardous Materials*. 2006;**133**(1–3): 61–67. DOI: 10.1016/j.jhazmat.2004.12.041
- [16] Ruzmanova Y, Ustundas M, Stoller M, Chianese A. Photocatalytic treatment of olive mill wastewater by N-doped titanium dioxide nanoparticles under visible light. *Chemical Engineering Transactions*. 2013: 2233–2238
- [17] Vaiano V, Sacco O, Stoller M, Chianese A, Ciambelli P, Sannino D. Influence of the photoreactor configuration and of different light sources in the photocatalytic treatment of highly polluted wastewater. *International Journal of Chemical Reactor Engineering*. 2014
- [18] Cicci A, Stoller M, Bravi M. Microalgal biomass production by using ultra- and nanofiltration membrane fractions of olive mill wastewater. *Water Research*. 2013;**47**(13): 4710–4718. DOI: 10.1016/j.watres.2013.05.030
- [19] Stoller M, Bravi M. Critical flux analyses on differently pretreated olive vegetation waste water streams: Some case studies. *Desalination*. 2010;**250**(2): 578–582. DOI: 10.1016/j.desal.2009.09.027
- [20] Stoller M, De Caprariis B, Cicci A, Verdone N, Bravi M, Chianese A. About proper membrane process design affected by fouling by means of the analysis of measured threshold flux data. *Separation and Purification Technology*. 2013;**114**(0):83–89. DOI: 10.1016/j.seppur.2013.04.041
- [21] Stoller M, Bravi M, Chianese A. Threshold flux measurements of a nanofiltration membrane module by critical flux data conversion. *Desalination*. 2013;**315**:142–148. DOI: 10.1016/j.desal.2012.11.013
- [22] Stoller M. On the effect of flocculation as pretreatment process and particle size distribution for membrane fouling reduction. *Desalination*. 2009; **240**(1–3):209–217. DOI: 10.1016/j.desal.2007.12.042
- [23] Bhaumik M, Setshedi K, Maity A, Onyango MS. Chromium(VI) removal from water using fixed bed column of polypyrrole/Fe₃O₄ nanocomposite. *Separation and Purification Technology*. 2013;**110**:11–19. DOI: 10.1016/j.seppur.2013.02.037.
- [24] Zahra S, Reyhane S, Reza F. Fixed-bed adsorption dynamic of Pb(II) adsorption from aqueous solution using nanostructured γ -alumina. *Journal of Nanostructure in Chemistry*. 2013:1–8
- [25] Setshedi KZ, Bhaumik M, Onyango MS, Maity A. Breakthrough studies for Cr(VI) sorption from aqueous solution using exfoliated polypyrrole-organically modified montmorillonite clay nanocomposite. *Journal of Industrial and Engineering Chemistry*. 2014;**20**(4):2208–2216. DOI: 10.1016/j.jiec.2013.09.052
- [26] Thomas H. Heterogeneous ion exchange in a flowing system. *Journal of the American Chemical Society*. 1944: 1466–1664
- [27] Yoon Y, Nelson J. Application of gas adsorption kinetics. I. a theoretical model for respirator cartridge service time. *American Industrial Hygiene Association Journal*. 1984:509–516
- [28] Tonle KI. Capteurs Électrochimiques à Base d'argiles Smectitiques Camerounaises Fonctionnalisées Par Les Groupements Thiol et Amine: Élaboration, Caractérisation et Application Au Piégeage Des Métaux Lourds à Effet

Polluant [These]. Yaoundé, Cameroun: Université de Yaoundé 1; 2004

[29] Brunaeur S, Deming LS, Deming WE, Teller E. On a theory of the Van Der Waals adsorption of gases. *Journal of the American Chemical Society*. 1940;1723

[30] Sing KSW, Everett DH, Haul RAW. Reporting physisorption data for gas/solid systems with special reference to the determination of surface area and porosity. *Pure and Applied Chemistry*. 1985;603

[31] Ofomaja AE, Ho Y-S. Effect of temperatures and PH on methyl violet biosorption by *Mansonia* wood sawdust. *Bioresource Technology*. 2008;99(13): 5411-5417. DOI: 10.1016/j.biortech.2007.11.018

[32] Liang Q-Q, Li Y-S. A rapid and accurate method for determining protein content in dairy products based on asynchronous-injection alternating merging zone flow-injection spectrophotometry. *Food Chemistry*. 2013;141(3):2479-2485. DOI: 10.1016/j.foodchem.2013.05.075

[33] Wang J, Zhang Q-H, Wang Z-H, Lih H-M. Determination of major bovine milk proteins by reversed-phase high-performance liquid chromatography. *Chinese Journal of Analytical Chemistry*. 2009: 1667-1670

[34] Aksu Z, Gönen F. Biosorption of phenol by immobilized activated sludge in a continuous packed bed: Prediction of breakthrough curves. *Process Biochemistry*. 2004;39(5): 599-613. DOI: 10.1016/S0032-9592(03)00132-8

[35] Calero M, Hernainz F, Blazquez G, Tenorio G, Martin-Lara MA. Study of Cr (III) biosorption in a fixed-bed column. *Journal of Hazardous Materials*. 2009: 886-893

[36] Yahaya N, Khan EM, Abustan I, Muhamad Faizal Pakir ML, Olugbenga SB, Mohd AA. Fixed-bed column study for Cu (II) removal from aqueous solutions using rice husk based activated carbon. *International Journal of Engineering and Technology*. 2011: 186-190

[37] Sivakumar P, Palanisamy PN. Packed bed column studies for the removal of acid blue 92 and basic red 29 using non-conventional adsorbent. *Indian Journal of Chemical Technology*. 2009;301-307

[38] Ochando-Pulido JM, Stoller M, Bravi M, Martinez-Ferez A, Chianese A. Batch membrane treatment of olive vegetation wastewater from two-phase olive oil production process by threshold flux based methods. *Separation and Purification Technology*. 2012;101(0):34-41. DOI: 10.1016/j.seppur.2012.09.015

[39] Bendini A, Cerretani L, Carrasco-Pancorbo A, Maria Gómez-Caravaca A, Segura-Carretero A, Fernández-Gutiérrez A, et al. Phenolic molecules in virgin olive oils: A survey of their sensory properties, health effects, antioxidant activity and analytical methods. *Molecules*. 2007;12(12): 1679-1719

[40] Soto ML, Moure A, Domínguez H, Parajó JC. Recovery, concentration and purification of phenolic compounds by adsorption: A review. *Journal of Food Engineering*. 2011;105(1):1-27. DOI: 10.1016/j.jfoodeng.2011.02.010

[41] Streat M, Sweetland LA. Removal of pesticides from water using hypercrosslinked polymer phases: Part 1-physical and chemical characterization of adsorbents. *Transactions of the Institution of Chemical Engineers*. 1998;B76:115-126

[42] Azonova VV, Hradil J. Sorption properties of macroporous and

Hyperscrosslinked copolymers. Reactive and Functional Polymers. 1999:163-175

[43] Maity N, Payne GF, Chipchosky JL. Adsorptive separations based on the differences in solute-sorbent hydrogen-bonding strengths. Industrial and Engineering Chemistry Research. 1991: 2456-2463

[44] Juang RS, Shiau JY. Effect of temperature on equilibrium adsorption of phenols onto nonionic polymeric resins. Separation Science and Technology. 1999:1819-1831

[45] Weber WJ Jr, Van Vliet BM. Synthetic adsorbents and activated carbons for water treatment: Overview and experimental comparisons. Journal of the American Chemical Society. 1981: 420-426

[46] Li C, Xu M, Sun X, Han S, Wu X, Liu Y-N, et al. Chemical modification of amberlite XAD-4 by carbonyl groups for phenol adsorption from wastewater. Chemical Engineering Journal. 2013; **229**:20-26. DOI: 10.1016/j.cej.2013.05.090